Date: February 15, 2008
Version: 1.5.2
Editors: Zuzana Rúriková, Juraj Braciník, Günter Grindhammer
Referees: Karin Daum, Katja Krueger (previously Sebastian Schmidt)
Deadline for comments: Feb. 29, 2008

Study of Charm Fragmentation into $D^{*\pm}$ Mesons in Deep-Inelastic Scattering at HERA

H1 Collaboration

Abstract

The process of charm fragmentation is studied using $D^{*\pm}$ meson production in deep-inelastic scattering as measured by the H1 detector at HERA. Two different methods are used for the definition of the observable approximating the fraction of the four-momentum of the $D^{*\pm}$ meson with respect to the charm quark. The momentum of the charm quark is approximated in the $\gamma^{*}p$-rest-frame either by the momentum of the jet including the $D^{*\pm}$ meson or by the momentum of a hemisphere which includes the $D^{*\pm}$ meson. The parameters of fragmentation functions are extracted using two QCD models based on leading order matrix elements and DGLAP or CCFM evolution of partons together with string fragmentation and particle decays. Additionally, they are determined for a next-to-leading order QCD calculation in the fixed flavour number scheme.

To be submitted to *Eur. Phys. J.* **C**

1 Introduction

The production of charm quarks is expected to be well described by perturbative QCD (pQCD) calculations due to the hard scale provided by the charm mass. The evolution of an "off-shell" charm quark via gluon radiation until it is "on-shell" can be calculated in pQCD in fixed order of the strong coupling or by summing all orders in the leading-log approximation. The transition of an on-shell charm quark into a charmed hadron is however not calculable within the framework of pQCD and is thus usually described by phenomenological models. One of the major characteristics of this transition process is the momentum fraction transferred from the quark to the hadron, which is parametrised by a fragmentation function.

There are several phenomenological models available, which describe the transition of a quark into hadrons, for example the independent fragmentation [1] and the string model [2]. The fragmentation function is defined in the context of a phenomenological model together with a pQCD calculation. Only if this context is fixed, is universality expected to hold, i.e. a fragmentation function extracted from experimental data of a given process can be used for predictions of different processes.

The fragmentation function is not a directly measurable quantity as the momentum of the heavy quark is experimentally not directly accessible. Also the momentum distribution of the heavy hadron can be only measured within certain limitations. Typically, the measurement cannot be performed over the whole phase space of the produced heavy hadron. The momentum spectrum is further distorted by heavy hadrons which are not produced directly, but are the result of decays of higher excited heavy hadrons, whose contribution is not well known.

The production of charmed hadrons has been measured in e^+e^- annihilation experiments, and parameters of fragmentation functions have been determined [3–10]. The H1 and ZEUS collaborations have published total cross sections for the production of various charmed hadrons in deep-inelastic ep scattering (DIS) [11] and in photoproduction [12]. These data show that the probabilities of charm quarks to fragment into various final state hadrons are consistent within experimental uncertainties for e^+e^- and ep collisions.

In this paper the transition of a charm quark into a $D^{*\pm}$ meson in DIS is further investigated. The normalised differential cross sections as a function of two observables with different sensitivity to gluon emissions are measured. The momentum of the charm quark is in one case approximated by the momentum of the jet which includes the $D^{*\pm}$ meson and in the other case by the momentum of a suitably defined hemisphere containing the $D^{*\pm}$ meson. The measurement is performed in the phase space, defined by the photon virtuality $2 < Q^2 < 100$ GeV^2, the inelasticity $0.05 < y < 0.7$, the transverse momentum of the $D^{*\pm}$ meson $1.5 < P_{\mathrm{T}}(D^{*\pm}) < 15$ GeV and the pseudorapidity $|\eta(D^{*\pm})| < 1.5$. In addition, the presence of a jet with $E^*_{\mathrm{T}} > 3$ GeV in the γ^*p-rest-frame [1], containing the $D^{*\pm}$ meson, is required.

The resultant normalised differential cross sections are used to fit parameters of two different fragmentation functions within QCD models as implemented in the Monte Carlo (MC) programs RAPGAP/PYTHIA [13, 14] and CASCADE/PYTHIA [15], and for the next-to-leading order (NLO) QCD calculation as implemented in HVQDIS [16].

[1] Variables with the superscript * refer to the rest-frame of the virtual photon (γ^*) and proton.

The paper is organised as follows. In section 2 a brief description of the H1 detector is given. It is followed by the details of the event selection, the $D^{*\pm}$ meson signal extraction and the jet finding and selection in section 3. The experimental fragmentation observables are defined in section 4. The QCD models and calculations used for data corrections and for the extraction of fragmentation functions are described in section 5. The data correction procedure and the determination of systematic uncertainties is explained in section 6. Finally, in section 7 the results of the measurements and of the fits of the fragmentation parameters are given.

2 H1 Detector

The data were collected with the H1 detector at HERA in the years 1999 and 2000. During this period HERA collided positrons of energy $E_e = 27.5$ GeV with protons of energy $E_p = 920$ GeV corresponding to a centre-of-mass energy of $\sqrt{s} = 319$ GeV. The data sample used for this analysis corresponds to an integrated luminosity of 47 pb^{-1}.

A detailed description of the H1 detector can be found in [17]. Here only the relevant components for this analysis are described. A right handed Cartesian coordinate system is used with the origin at the nominal primary ep interaction vertex. The direction of the proton beam defines the positive z-axis (forward direction). Transverse momenta are measured in the x-y plane. Polar (θ) and azimuthal (ϕ) angles are measured with respect to this reference system. The pseudorapidity is defined as $\eta = -\ln\tan\frac{\theta}{2}$.

The scattered positron is identified and measured in the SpaCal calorimeter [18], a lead-scintillating fibre calorimeter situated in the backward region of the H1 detector, covering the polar angular range $-4.0 < \eta < -1.4$. Hits in the backward drift chamber (BDC) are used to improve the identification of the scattered positron and the measurement of its angle. Charged particles emerging from the interaction region are measured by the Central Silicon Track detector (CST) [19] and the Central Tracking Detector (CTD), which covers a range $-1.74 < \eta < 1.74$. The CTD comprises two large cylindrical Central Jet drift Chambers (CJCs) and two z-chambers situated concentrically around the beam-line within a solenoidal magnetic field of 1.16 T. The CTD also provides triggering information based on track segments measured in the r-ϕ-plane of the CJCs and on the z-position of the event vertex obtained from the double layers of two Multi-Wire Proportional Chambers (MWPCs). In the central and forward region the track detectors are surrounded by a finely segmented Liquid Argon calorimeter (LAr) [20]. It consists of an electromagnetic section with lead absorbers and a hadronic section with steel absorbers and covers the range $-1.5 < \eta < 3.4$.

The luminosity determination is based on the measurement of the Bethe-Heitler process ($ep \rightarrow ep\gamma$), where the photon is detected in a calorimeter close to the beam pipe at z=-103 m.

3 Data Selection and Analysis

The events selected in this analysis are required to contain a scattered positron in the SpaCal and at least one $D^{*\pm}$ meson candidate, as reconstructed from tracks measured with the CST and CTD. The scattered positron is required to have an energy above 8 GeV. The virtuality of the photon Q^2, as well as the inelasticity y of the event and the boost to the $\gamma^* p$-rest-frame are determined from the measured energy and polar and azimuthal angle of the positron. In addition, this analysis makes use of the $\gamma^* p$ centre-of-mass energy W:

$$Q^2 = 4E_e E'_e \cos^2\left(\frac{\Theta_e}{2}\right) \qquad y = 1 - \frac{E'_e}{E_e}\sin^2\left(\frac{\Theta_e}{2}\right)$$
$$W^2 = ys - Q^2 \ , \tag{1}$$

where $s = 4E_e E_p$, and E_e and E_p denote the energies of the incoming positron and proton, respectively. The photon virtuality is required to be in the range $2 < Q^2 < 100$ GeV^2. This kinematic range is determined by the geometric acceptance of the SpaCal. The inelasticity of the event is required to lie in the region $0.05 < y < 0.7$. The difference between the total energy E and the longitudinal component of the total momentum P_z, as calculated from the scattered positron and the hadronic final state, is restricted to $40 < E - P_\mathrm{z} < 75$ GeV. This requirement suppresses photoproduction background, where a hadron is misidentified as the scattered positron. It also reduces the contribution of DIS events with initial state photon radiation for which the escaped positron or photon in the $-z$-direction leads to values of $E - P_\mathrm{z}$ lower than the expectation $2E_e = 55$ GeV.

The $D^{*\pm}$ mesons are reconstructed using the decay channel $D^{*\pm} \rightarrow \overset{(-)}{D^0}\ \pi_\mathrm{s}^\pm \rightarrow (K^\mp\pi^\pm)\pi_\mathrm{s}^\pm$, where π_s denotes the low momentum pion from the $D^{*\pm}$ meson decay. Requirements on the transverse momentum and pseudorapidity of the $D^{*\pm}$ meson candidate and its decay products as well as on particle identification using $\mathrm{d}E/\mathrm{d}x$ are very similar to those used in previous H1 analyses [21]. A summary of the kinematic requirements is given in table 1.

D^0	$P_\mathrm{T}(K,\pi) > 0.25$ GeV $P_\mathrm{T}(K) + P_\mathrm{T}(\pi) > 2$ GeV $\lvert M(K\pi) - M(D^0)\rvert < 0.07$ GeV
$D^{*\pm}$	$P_\mathrm{T}(\pi_\mathrm{s}) > 0.12$ GeV $\lvert\eta(D^{*\pm})\rvert < 1.5$ $1.5 < P_\mathrm{T}(D^{*\pm}) < 15$ GeV

Table 1: Kinematic requirements for the selection of $D^{*\pm}$ meson candidates.

To select $D^{*\pm}$ meson candidates the mass difference $\Delta M_{D^{*\pm}} = M(K\pi\pi_\mathrm{s}) - M(K\pi)$ [22] is used. Its distribution for the full data sample is shown in figure 1 together with the wrong charge $K^\pm\pi^\pm\pi_\mathrm{s}^\mp$ combinations, using $K^\pm\pi^\pm$ pairs in the accepted D^0 mass range. The wrong charge $\Delta M_{D^{*\pm}}$ distribution provides a good description of the right charge combinatorial background and is thus used to stabilise the fit of the background in the signal region.

The signal is extracted using a simultaneous fit to the $\Delta M_{D^{*\pm}}$ distribution of the right and wrong charge combinations. The signal is fitted using a modified Gaussian function

$$G_\mathrm{mod} \propto N_{D^{*\pm}}\ \exp\left[-0.5\, x^{1+1/(1+0.5\,x)}\right] \ ,$$

where $x = |\Delta M_{D^{*\pm}} - M_0|/\sigma$. The signal position M_0 and width σ as well as the number of $D^{*\pm}$ mesons $N_{D^{*\pm}}$ are free parameters of the fit. The background is parametrised as a power function of the form $N/(a+1)\,(\Delta M_{D^{*\pm}} - m_\pi)^a/(M - m_\pi)^{a+1}$. The two free parameters a and N determine the shape and normalisation of the background. First, the total event sample is fitted using six free parameters, i.e. three for the modified Gaussian, two for the normalisation of the right and wrong charge $\Delta M_{D^{*\pm}}$ distributions and one for the background shape, common for the right and wrong charge combinatorial background. The number of $D^{*\pm}$ mesons in the total sample is 2865 ± 89 (stat.). The number of $D^{*\pm}$ mesons in the measurement bins shown in figures 3-9 is extracted using the same procedure, except that a four parameter fit is performed with the position of the signal peak and its width fixed to the values determined from the fit to the full sample.

The hadronic final state is reconstructed in each event using an energy flow algorithm. It combines charged particle tracks and calorimetric energy clusters, taking into account their respective resolution and geometric overlap, into so called hadronic objects while avoiding double counting of energy. The three hadronic objects, corresponding to the three decay tracks forming the $D^{*\pm}$ meson, are removed from the event and replaced by the four-momentum vector of the reconstructed $D^{*\pm}$ meson candidate.

Jets are found in the $\gamma^* p$-rest-frame using the inclusive k_T cluster algorithm [23] with distance parameter $R = 1$ in the η-ϕ plane. To combine hadronic objects into jets, the E-recombination scheme is applied, in which the four-momenta of the objects are used. For the $D^{*\pm}$ meson mass the nominal value is used. The jet containing the $D^{*\pm}$ meson candidate is referred to as $D^{*\pm}$ jet and is required to satisfy the condition $E_\mathrm{T}^* > 3$ GeV in the $\gamma^* p$-rest-frame. This rather low jet transverse momentum requirement allows to collect a large sample of $D^{*\pm}$ mesons, which are mainly produced at low P_T as a consequence of the $c\bar{c}$ production enhancement near threshold. Nevertheless, according to MC simulations, the $D^{*\pm}$ jet is found to be well correlated with the originating charm or anti-charm quark. The distance in azimuth-pseudorapidity, $\Delta r = \sqrt{\Delta\eta^2 + \Delta\phi^2}$, between the charm quark jet found using final state partons and the $D^{*\pm}$ jet found using final state hadrons is below 0.3 for 90% of all cases. The correlation between hadron and detector level is even better, since most of the energy of low E_T^* jets can be reconstructed from tracks which are well measured in the tracking system. The number of $D^{*\pm}$ mesons in the sample of events with a $D^{*\pm}$ jet is 1508 ± 68 (stat.).

4 Definition of Experimental Observables

A convenient method to study fragmentation is to measure the differential cross section of a heavy hadron (H) as a function of a scaled momentum or energy z. In e^+e^- experiments a customary experimental definition is $\mathrm{z}_{\mathrm{e^+e^-}} = E_\mathrm{H}/E_\mathrm{beam}$, where E_beam is the energy of the beams in the centre-of-mass system. In leading order, i.e. without gluon emissions, the beam energy is also equal to the energy of the charm or anti-charm quark, which are produced in a colour singlet state. The differential cross section of heavy hadron production as a function of z is directly related to the fragmentation function.

In the case of ep interactions, the situation is more complex. In DIS the dominant process for $D^{*\pm}$ meson production occurs via boson-gluon fusion $\gamma^* g \to c\bar{c}$ (BGF) [21]. In this case the $c\bar{c}$ pair is produced in a colour octet state. The energy of the charm quarks depends on the energy of the incoming photon and gluon. Hadrons produced by initial state gluon emissions and by fragmentation of the proton remnant are also present in the final state. Final state gluon radiation occurs of course in e^+e^- as well as in ep interactions.

In this analysis two methods to study the fragmentation function are used by measuring the differential cross sections of $D^{*\pm}$ mesons as a function of two different observables, related to the fraction of momentum inherited by the $D^{*\pm}$ meson from the initial charm quark.

The hemisphere method: $\mathbf{z=z_{hem}}$

An illustration of the hemisphere method is shown in figure 2. In the leading order BGF process, dominating charm production at HERA, the charm and anti-charm quarks are moving in the direction of the virtual photon in the $\gamma^* p$-rest-frame of reference. This is due to the fact that the photon is on average more energetic than the gluon, which typically carries only a small fraction of the proton's momentum. Assuming no further gluon radiation in the initial and final state, the charm and anti-charm quarks are balanced in transverse momentum (figure 2, left). This observation suggests to divide the event into two hemispheres, one containing the fragmentation products of the charm quark, the other one those of the anti-charm quark. In order to suppress contributions from initial state radiation and the proton remnant, particles pointing in the proton direction, i.e. particles with $P^*_{\mathrm{z}} < 0$ are discarded (the photon direction is taken as as the direction of the z-axis in the $\gamma^* p$-rest-frame). The projections of the momenta of the remaining particles onto a plane perpendicular to the $\gamma^* p$-axis are determined. Using the projected momenta, the thrust-axis in this plane, i.e. the axis maximising the sum of the longitudinal momenta of these particles along this axis, is found. A line perpendicular to the thrust-axis allows to divide the projected event into two hemispheres, one of them containing the $D^{*\pm}$ meson and usually other particles (figure 2, right). The particles that belong to the same hemisphere as the $D^{*\pm}$ meson are attributed to the fragmentation of the charm or anticharm quark. The fragmentation observable is thus defined as:

$$\mathrm{z_{hem}} = \frac{(E^* + P^*_{\mathrm{L}})_{D^{*\pm}}}{\sum_{\mathrm{hem}}(E^* + P^*)} \,, \tag{2}$$

where in the denominator the energy and momentum of all particles of the $D^{*\pm}$ meson hemisphere are summed. The longitudinal momentum $P^*_{\mathrm{L}\,D^{*\pm}}$ is defined with respect to the direction of the three-momentum of the hemisphere, defined as a sum of three-momenta of all particles belonging to the hemisphere.

The jet method: $\mathbf{z=z_{jet}}$

In the case of the jet method the energy and direction of the charm quark are approximated by the energy and direction of the reconstructed jet which contains the $D^{*\pm}$ meson. The fragmentation observable is defined as:

$$z_{\mathrm{jet}} = \frac{(E^* + P^*_{\mathrm{L}})_{D^{*\pm}}}{(E^* + P^*)_{\mathrm{jet}}} \ , \tag{3}$$

where the longitudinal momentum $P^*_{\mathrm{L}\,D^{*\pm}}$ is defined with respect to the direction of the three-momentum of the jet. The jet finding and the determination of z_{jet} are performed in the $\gamma^* p$-rest-frame.

These fragmentation observables are defined in such a way that, assuming no gluon radiation and independently fragmenting charm quarks, they would lead to similar distributions. The measured distributions, however, are expected to differ, as they have different sensitivity to gluon radiation and charm quarks which do not fragment independently. The hemisphere method typically includes more energy around the charm quark direction than the jet method. The parameters of fragmentation functions however, if extracted with QCD models which provide a very good description of the underlying physics over the full phase space of this analysis, should be the same. A comparison of both methods thus may provide a consistency check or a test of the perturbative and non-perturbative physics as encoded in the models.

In order to minimise the sensitivity of the analysis to the total $D^{*\pm}$ meson cross section, and to reduce systematic errors, shape normalised differential cross sections as a function of the fragmentation observables z_{hem} and z_{jet} are measured. The z_{hem} and z_{jet} distributions are normalised to unity in the respective z-region, where the measurement can be performed, i.e. $0.2 < z_{\mathrm{hem}} \leq 1.0$ and $0.3 < z_{\mathrm{jet}} \leq 1.0$.

5 QCD Models

QCD models are used to generate events containing charm and beauty quarks, which are then passed through a detailed simulation of the detector response, based on the GEANT simulation program [24], and are reconstructed using the same software as used for the data. The obtained event samples are used to determine the acceptance and efficiency and to estimate the systematic errors associated with the measurements. Fitting these models to data, the parameters of the underlying fragmentation functions are determined.

The Monte Carlo program RAPGAP [13], based on collinear factorisation and DGLAP [25] evolution, is used to generate the direct process of photon-gluon fusion to a heavy (charm or beauty) quark anti-quark pair, where the photon acts as a point-like object. In addition, RAPGAP allows the simulation of charm production via resolved processes, where the photon fluctuates into partons, one of which interacts with a parton in the proton, and the remaining partons produce a photon remnant. The program uses LO matrix elements with massive (massless) charm quarks for the direct (resolved) processes. Parton showers based on DGLAP evolution are used to model higher order QCD effects.

The CASCADE program [15] is based on the k_{T}-factorisation approach. In the $\gamma^* g \to c\bar{c}$ matrix element the charm mass is taken into account, but also the fact that the incoming gluon is off mass-shell and can have a finite transverse momentum. Parton showers off the charm or anti-charm quark are implemented including angular ordering constraints. The incoming gluon density is evolved according to the CCFM equations [26]. The k_{T}-unintegrated gluon density function is used as obtained from an analysis of inclusive DIS data [27].

In both RAPGAP and CASCADE the hadronisation of partons is performed using the Lund string model as implemented in PYTHIA [14]. In the Lund model, the heavy hadron is produced in the process of string breaking. The fraction of the string longitudinal momentum carried by the hadron is generated according to different choices of adjustable fragmentation functions. Within this analysis three widely used parametrisations are employed, two of them depend on a single free parameter, and one depends on two free parameters. The parametrisation suggested by Peterson et al. [28] has the functional form:

$$D_{\mathrm{Q}}^{\mathrm{H}}(z) \propto \frac{1}{z[1-(1/z)-\varepsilon/(1-z)]^2} \tag{4}$$

and the one by Kartvelishvili et al. [29] is given by:

$$D_{\mathrm{Q}}^{\mathrm{H}}(z) \propto z^{\alpha}(1-z). \tag{5}$$

The free parameters ε and α determine the "hardness" of the fragmentation function and are specific to the flavour of the heavy quark, i.e. charm in case of $D^{*\pm}$ meson production. The parametrisation inspired by Bowler and Morris [30] (referred to as Bowler parametrisation) has the functional form:

$$D_{\mathrm{Q}}^{\mathrm{H}}(z) \propto \frac{1}{z^{1+r_Q b m_Q^2}}(1-z)^a \exp\left(-\frac{bM_{\mathrm{T}}^2}{z}\right). \tag{6}$$

The shape of the fragmentation function is determined by two free parameters a and b, m_Q is the mass of the heavy quark, $M_{\mathrm{T}} = \sqrt{M^2 + P_{\mathrm{T}}^2}$ the transverse mass of the heavy hadron, and $r_Q = 1$ as default in PYTHIA.

For correcting data, the parameter setting tuned by the ALEPH collaboration [31] is used for the fragmentation of partons in PYTHIA. It includes higher excited charm states of which some also decay to $D^{*\pm}$ mesons and contribute significantly to the $D^{*\pm}$ meson yield. When extracting fragmentation functions also the default parameter set of PYTHIA with the Peterson fragmentation function is used as an alternative. In this case no higher excited charm states are produced. Both parameter settings are indicated in table 4.

The HVQDIS program [16] is also used to extract parameters for the Kartvelishvili and Peterson fragmentation functions. It is based on the full NLO, i.e. $\mathcal{O}(\alpha_{\mathrm{s}}^2)$, calculation in the fixed flavour number scheme, with three light active flavours and the gluon in the proton. The proton PDFs of the light quarks and the gluon are evolved according to the DGLAP equations. Massive charm (or beauty) quarks are assumed to be produced only perturbatively via photon-gluon fusion and higher-order processes. The final state charm quarks are fragmented independently into $D^{*\pm}$ mesons in the $\gamma^* p$-rest-frame. The Kartvelishvili or Peterson parametrisations are used to generate the fraction of the c-quark's momentum transferred to the $D^{*\pm}$ meson. Its energy is calculated using the on-mass-shell condition. In addition, to account for possible P_{T} smearing of the $D^{*\pm}$ meson, it can be given a transverse momentum P_{T} with respect to the charm quark, according to the function $P_{\mathrm{T}} \exp(-\beta P_{\mathrm{T}})$. The value used for the parameter β corresponds to $< P_{\mathrm{T}} > = 350$ MeV [21].

The Monte Carlo programs RAPGAP and HERWIG [32] are used to estimate the size of the hadronisation corrections. While the perturbative QCD model of HERWIG is similar to the one of RAPGAP, the HERWIG program employs the cluster hadronisation model, which is quite different from the Lund string model used by PYTHIA.

The basic parameter choices for various Monte Carlo and NLO programs are summarised in table 2.

	RAPGAP	**CASCADE**	**HERWIG**	**HVQDIS**
proton PDF	CTEQ5L [33]	A0 [27]	CTEQ5L [33]	CTEQ5F3 [33]
photon PDF	SaSD-2D [34]		SaSG-1D [34]	
μ	$\sqrt{Q^2 + P_{\mathrm{T}}^2}$	$\sqrt{4m_c^2 + P_{\mathrm{T}}^2}$	$\sqrt{\hat{s}}$	$\sqrt{Q^2 + 4m_c^2}$
m_c [GeV]	1.5	1.5	1.5	1.5
fragmentation model	Lund string	Lund string	cluster	independent

Table 2: Parton density functions (PDFs), fragmentation models and basic parameters used in the Monte Carlo and NLO programs. The renormalisation and factorisation scales are set equal, $\mu = \mu_{\mathrm{r}} = \mu_{\mathrm{f}}$ (apart from CASCADE where $\mu_{\mathrm{f}} = \sqrt{\hat{s} + Q_{\mathrm{T}}^2}$; here the invariant mass squared and the transverse momentum squared of the $c\bar{c}$-pair are denoted by $\hat{s}$ and Q_{T}^2, respectively), and m_c is the charm quark mass.

6 Data Corrections and Systematic Errors

The data are corrected for detector and QED radiative effects. The small contribution of $D^{*\pm}$ mesons originating from B-hadron decays is estimated with RAPGAP and is subtracted from the data. It is less than 2%. The transverse momentum and pseudorapidity distributions of the $D^{*\pm}$ mesons of the Monte Carlo events are reweighted simultaneously to those of the data in order to achieve an improved description. The η and P_{T} reweighting factors applied differ from unity by typically $10 - 30\%$. After this reweighting, both MC models and the detector simulation provide a good description of the data as shown in figure 3. The purity of the bins of the hemisphere and the jet sample, defined as the fraction of events reconstructed in a $\mathrm{z}_{\mathrm{hem}}$ or $\mathrm{z}_{\mathrm{jet}}$ bin that originate from that bin on hadron level, is found to vary between 40 and 70%, mainly driven by the resolution in z. Correction for the detector effects is done using regularised deconvolution, taking into account migrations between measurement bins [35]. The detector response matrix is generated using RAPGAP, and the value of the regularisation parameter is determined using decomposition of the data into eigenvectors of the detector response matrix. Statistical errors are calculated by error propagation using the covariance matrix, assuming that statistical errors on detector level are not correlated between bins. The data are then corrected for migrations from and into the visible phase space using RAPGAP and CASCADE. The effects of QED radiation are corrected for using the HERACLES [36] program which is interfaced with RAPGAP. Correction factors are calculated from the ratio between cross section obtained from the model including and not including QED radiation. The corrections are applied bin-by-bin in $\mathrm{z}_{\mathrm{hem}}$ or $\mathrm{z}_{\mathrm{jet}}$.

The HVQDIS program provides a full partonic final state and additionally the $D^{*\pm}$ meson. While the quantity $(E^* + P_{\mathrm{L}}^*)_{D^{*\pm}}$ in equation 2 and 3 is calculated using the momentum of the $D^{*\pm}$ meson, the jet finding and the calculation of hemisphere quantities, denominators in equations 2 and 3, are performed using the partonic final state. In order to compare the measured cross sections with HVQDIS predictions, hadronisation corrections are applied to the data. They are estimated by comparing the parton and hadron level cross sections of RAPGAP and HERWIG. All partons of RAPGAP and HERWIG after the parton shower step are considered, and the same jet and hemisphere finding algorithms are applied at parton and hadron level. For each z-bin the hadronisation correction factor is calculated as the ratio of parton to hadron level cross section. The arithmetic mean of the hadronisation correction factors of both models is used to multiply the data cross section. In case of $\mathrm{z_{hem}}$ the hadronisation corrections differ from unity by typically 40%. For $\mathrm{z_{jet}}$ they differ from unity by typically 20%, except for the highest z-bin, where they differ from unity by 50%.

The following sources of systematic errors on the differential cross sections are considered:

- The energy of the scattered positron is varied by $\pm 3\%$ for an energy of 8 GeV and by $\pm 1\%$ for 27 GeV. For intermediate energies the size of the variation is linearly dependent on energy.
- The polar angle of the scattered positron is varied by its estimated uncertainty of ± 1 mrad.
- To estimate the effect of the uncertainty of the energy scale of hadronic objects, the energies of tracks are varied by $\pm 0.5\%$, of clusters in LAr by $\pm 4\%$ and in SpaCal by $\pm 7\%$.
- The effect of the tracking efficiency uncertainty on reconstructing the $D^{*\pm}$ meson is estimated by changing the nominal efficiency in the simulation as a function of track η and P_{T}. In the corners of the accepted η, P_{T} phase space it is varied by $\pm 4\%$, and in the main region by $\pm 2\%$.
- The value of $\mathrm{d}E/\mathrm{d}x$ of the $D^{*\pm}$ meson decay products is varied in MC by $\pm 8\%$, which corresponds to the experimental resolution in $\mathrm{d}E/\mathrm{d}x$.
- Different procedures are applied to extract the $D^{*\pm}$ meson signal. The number of $D^{*\pm}$ mesons is determined from the parameters of the fit and from counting the entries above the fitted background in the signal region.
- The nominal cross section of beauty production of the RAPGAP MC is increased by a factor of 2. This reflects the fact that its predictions tend to underestimate the measured beauty cross section.
- The effect of using different MC models for the small correction of migrations from and into the visible phase space is studied using RAPGAP and CASCADE. The average correction factors are determined from the two models and are used to correct the data. Half of the difference is taken as systematic error.
- For parton level corrected distributions half of the difference between the hadronisation correction factors of RAPGAP and HERWIG is taken as the uncertainty due to the different fragmentation model, i.e. Lund string versus cluster model.

Other systematic errors which are investigated and found to be negligible are: the effect of reflections, i.e. wrongly or incompletely reconstructed $D^{*\pm}$ meson decays, on the shape of the fragmentation observables, the effect of including diffractive events on acceptance and reconstruction efficiency and the effect of using different MC models for the deconvolution of the data.

Each source of systematic error is varied in the Monte Carlo within its uncertainty. In each measurement bin, the corresponding deviation of the normalised cross sections from the central value is taken as systematic error. Among the systematic errors the uncertainties due to the scattered positron energy scale, the hadronic energy scale, and the beauty fraction are correlated amongst the bins in z. In the extraction of the parameters of the fragmentation functions, the uncorrelated as well as correlated statistical and systematic errors are taken into account. The average effect of various systematic errors on the $\mathrm{z}_{\mathrm{hem}}$ and $\mathrm{z}_{\mathrm{jet}}$ distributions is summarised in table 3. Since the distributions of $\mathrm{z}_{\mathrm{hem}}$ and $\mathrm{z}_{\mathrm{jet}}$ are shape-normalised, the effect of many systematic uncertainties is reduced such that the statistical error is dominating the measurement.

sources of systematic uncertainty	$\mathrm{z}_{\mathrm{hem}}$ error	$\mathrm{z}_{\mathrm{jet}}$ error
scattered positron energy scale	0.8%	0.5%
positron scattering angle	0.1%	0.1%
hadronic energy scale	3.0%	2.5%
track reconstruction efficiency	0.1%	0.1%
dE/dx measurement	0.1%	0.3%
$D^{*\pm}$ signal extraction	1.7%	1.7%
beauty fraction	1.2%	0.9%
model dependence of correction for migrations from and into the visible phase space	0.1%	0.3%
total systematic uncertainty	3.8%	3.4%
statistical uncertainty	9.5%	10.9%
uncertainty on corrections for hadronisation effects	3.9%	9.6%
total syst. uncertainty on data corrected for hadronisation effects	5.7%	10.6%

Table 3: Experimental and theoretical systematic uncertainties of the normalised z distributions, averaged over all bins. The last two entries in the table apply only when data are additionally corrected for hadronisation effects for comparison with HVQDIS.

7 Experimental Results

7.1 Normalised differential cross sections and comparison with different predictions

The normalised differential cross sections of $D^{*\pm}$ meson production as a function of the fragmentation observables $\mathrm{z}_{\mathrm{hem}}$ and $\mathrm{z}_{\mathrm{jet}}$ are shown in figure 4. They refer to the visible phase space given by $2 < Q^2 < 100$ GeV^2, $0.05 < y < 0.7$ and $1.5 < P_{\mathrm{T}}(D^{*\pm}) < 15$ GeV, $|\eta(D^{*\pm})| < 1.5$. In addition, a $D^{*\pm}$ jet with $E_{\mathrm{T}}^{*} > 3$ GeV in the $\gamma^* p$-rest-frame is required in order to have the same hard scale in the event for both distributions, $\mathrm{z}_{\mathrm{hem}}$ and $\mathrm{z}_{\mathrm{jet}}$. The measurements and the corresponding predictions are normalised to unity (see section 4). The striking difference between the two distributions observed in the highest $\mathrm{z}_{\mathrm{jet}}$ bin is mainly due to a significant fraction of $D^{*\pm}$ jets consisting of a $D^{*\pm}$ meson only, for which $\mathrm{z}_{\mathrm{jet}}$ equals unity. The normalised cross sections and their errors are given in table 5 for the hemisphere and in table 6 for the jet observable.

Figure 4 also includes predictions of RAPGAP with three commonly used fragmentation parameter settings for PYTHIA (see table 4), obtained from e^+e^- annihilation. The values of the corresponding χ^2/n.d.f., as calculated from the data and the model predictions, as well as the combination of parameter settings and corresponding values for the fragmentation function parameter used, are summarised in table 7. In general, there is reasonable agreement between data and the QCD model with all settings for both the jet and the hemisphere observable.

7.2 Extraction of parameters for the Kartvelishvili and Peterson fragmentation functions

The normalised $D^{*\pm}$ meson differential cross sections as a function of $\mathrm{z}_{\mathrm{hem}}$ and $\mathrm{z}_{\mathrm{jet}}$ are used to extract optimal parameters for the Peterson and Kartvelishvili fragmentation functions described in section 5.

The parameter extraction is done by comparing different model configurations to data. A configuration is defined by one of the QCD calculations (RAPGAP, CASCADE, or HVQDIS), by one of the fragmentation functions (Peterson or Kartvelishvili) and by a possible value for the corresponding fragmentation parameter, ε or α. In order to be able to compare all configurations to data, a reweighting procedure is applied. Large event samples with $D^{*\pm}$ mesons are generated for each of the three QCD calculations and for one fragmentation function. For these events the z-value of the fragmentation function used by the model to generate the fraction of charm quark (or string) momentum transferred to the $D^{*\pm}$ meson is stored such that each event can be reweighted to another fragmentation function or any other parameter value. For each configuration the predicted and measured distributions of the fragmentation observables are used to determine a χ^2 as a function of the fragmentation parameter. In the calculation of χ^2 the full covariance matrix is used, taking into account correlated and uncorrelated statistical and systematic errors. The best value of the fragmentation parameter is found at the minimum of χ^2. The shape of the χ^2 distribution (with $\chi^2_{\mathrm{min}} + 1$) is used to determine the $\pm 1\sigma$ error of the extracted parameter. As an example, in figure 5 the data are compared to the prediction of

RAPGAP using the ALEPH setting as given in table 4 and the Kartvelishvili parametrisation, with two lines indicating the $\pm 1\sigma$ total uncertainty around the best fit value of α.

The parameters α and ε, which are extracted using RAPGAP and CASCADE, with and without higher excited charmed hadrons, are summarised in table 8 together with their corresponding values of χ^2/n.d.f.. With the fitted parameters, the model predictions using either the Peterson or Kartvelishvili parametrisations describe the data reasonably well, as can be seen from the values of χ^2/n.d.f.. When using the same parameter settings, the fragmentation parameters extracted from the $\mathrm{z_{hem}}$ and $\mathrm{z_{jet}}$ observables are in good agreement. Both RAPGAP and CASCADE lead to statistically compatible parameters ε and α. A priori, agreement in the fragmentation function parameters for RAPGAP and CASCADE is not required, since the models differ in terms of simulated processes (direct and resolved in case of RAPGAP vs. direct only for CASCADE) and in their implementation of perturbative QCD.

The fragmentation parameters α and ε depend significantly on the parameter settings used, i.e. whether $D^{*\pm}$ mesons are assumed to be produced only via direct fragmentation of charm quarks or additionally originate from decays of higher excited charm states. In the latter case the $D^{*\pm}$-mesons carry a smaller fraction of the original charm or anti-charm quark momentum in comparison with the directly produced ones. Both the default settings and the settings containing higher excited charm states lead to a reasonable description of the data. The value of the Peterson parameter ε, extracted for the setting containing higher charm states, is in agreement with the value $\varepsilon = 0.04$ tuned by ALEPH, supporting the hypothesis of fragmentation universality between ep and e^+e^-. In an alternative method parameter values are determined by directly fitting Monte Carlo predictions at detector level to uncorrected data. The results obtained are found to be in very good agreement with our nominal procedure.

The NLO calculation as implemented in HVQDIS with the Kartvelishvili fragmentation function leads to a good fit of the data, while it fails to describe $\mathrm{z_{hem}}$ and also $\mathrm{z_{jet}}$ when the Peterson fragmentation function is used (see table 8 and figure 6). The effect of smearing the P_{T} of the $D^{*\pm}$ meson with respect to the charm quark on the extracted value of α is very small in both cases.

In order to study whether the Q^2 or W dependence of the fragmentation observables can be described by the QCD models using the fragmentation parameters obtained from the fits, the observables $\mathrm{z_{hem}}$ and $\mathrm{z_{jet}}$ are also measured in two bins in Q^2 ($2 < Q^2 < 10$ and $10 < Q^2 < 100$ GeV^2) and in W ($W < 170$ and $W \geq 170$ GeV). Correction factors and systematic uncertainties for these samples are determined in the same way as for the nominal samples. The data are compared to the QCD models with parameter settings including higher excited charm states and using the Kartvelishvili fragmentation function. For the low and high Q^2 bins the measured distributions are found to be almost the same and well described by the QCD models. The distribution of $\mathrm{z_{jet}}$ is also similar at low and high W. A difference is observed for the $\mathrm{z_{hem}}$ distribution, which is softer at high W as shown in figure 7. RAPGAP (and CASCADE) show the same behaviour as a function of W as observed in data. This behaviour can be understood as being partly due to the effect of the requirement $P_{\mathrm{T}}(D^{*\pm}) > 1.5$ GeV at low and high W and due to enhanced gluon radiation at high W.

The hemisphere observable allows to investigate the fragmentation of charm close to the kinematic threshold, at the limit of applicability of the concept of fragmentation function. A sample of events is selected with the nominal requirements on the DIS and $D^{*\pm}$ meson phase space and by requiring that there are no $D^{*\pm}$ jets with an $E_{\mathrm{T}}^{*} > 3$ GeV in an event. The event sample thus obtained has no overlap with the nominal sample investigated so far. It has similar statistics as the nominal event sample. A comparison of this data sample with the predictions of the QCD models at detector level is shown in figure 8. The sample without a $D^{*\pm}$ jet is found to be less well described than the nominal sample. The correction factors and systematic uncertainties for the $\mathrm{z}_{\mathrm{hem}}$ distribution for this sample are evaluated using the same procedure as for the nominal data sample. The normalised cross sections and errors are given in table 9 and are plotted together with the predictions of RAPGAP, showing the $\pm 1\sigma$ total uncertainty around the fitted value of α in figure 9. The fragmentation parameters are extracted for RAPGAP, CASCADE and the NLO calculation using the same procedure as for the nominal data sample and are summarised in table 10. The fragmentation parameters extracted for RAPGAP and CASCADE are statistically compatible. The NLO calculation as implemented in HVQDIS fails to describe the data sample without a $D^{*\pm}$ jet. Predictions of RAPGAP with the three commonly used fragmentation parameter settings for PYTHIA (see table 4), which provide a reasonable description of the data sample with a hard scale, fail for the sample close to the kinematic threshold.

The fragmentation parameters fitted to the data sample without a $D^{*\pm}$ jet are found to be significantly different from those for the nominal sample. They indicate that the fragmentation function for an optimal description of the sample without a $D^{*\pm}$ jet needs to be significantly harder (see figure 9) than the one for the nominal sample. The influence of several aspects of the QCD models on the result that different fragmentation parameters are required for the two data samples is studied. By, for example, tuning parameters of the parton shower, it is not possible to obtain consistent parameters for the two samples. In order to study the effect of diffractive charm events on the extracted parameters, diffractive events as generated by RAPGAP are added to its direct and resolved events. The fraction of diffractive events in the full sample is adjusted to achieve a good description of the tail of the $\eta_{\max}$ distribution [37]. The effect on the extracted parameters is found to be negligible. Therefore, the feature of requiring a significantly different fragmentation parameter for events close to the kinematic threshold can be considered as an inadequacy of both QCD models and possibly of the simple parametrisations used for the fragmentation function.

8 Conclusions

The fragmentation of charm quarks into $D^{*\pm}$ mesons in DIS is studied using the H1 detector at the HERA collider. The shape-normalised $D^{*\pm}$ meson differential cross sections as a function of two observables sensitive to fragmentation, the hemisphere observable $\mathrm{z}_{\mathrm{hem}}$ and the jet observable $\mathrm{z}_{\mathrm{jet}}$, are measured in the visible DIS phase space defined by $2 < Q^2 < 100$ GeV^2, $0.05 < y < 0.7$ and the $D^{*\pm}$ meson phase space $1.5 < P_{\mathrm{T}}(D^{*\pm}) < 15$ GeV, $|\eta(D^{*\pm})| < 1.5$. An additional $D^{*\pm}$ jet with $E_{\mathrm{T}}^{*} > 3$ GeV is required to provide a hard scale for the events.

The data are compared with predictions of QCD models with three widely used parameter settings and the Peterson and the Bowler parametrisation for the fragmentation of heavy flavours obtained from e^+e^- annihilation. They provide a reasonable description of the ep data presented.

The shape-normalised differential cross sections are used to extract parameters for the Kartvelishvili and Peterson fragmentation functions within the framework of the QCD models RAPGAP and CASCADE and the NLO QCD calculation as implemented in HVQDIS. The fragmentation parameters extracted using the $\mathrm{z_{hem}}$ and $\mathrm{z_{jet}}$ observables are in good agreement with each other. Both QCD models, RAPGAP and CASCADE, lead to statistically compatible parameters. The value of the Peterson parameter ε extracted for the parameter setting which includes not only $D^{*\pm}$ mesons from direct fragmentation of charm quarks but also from the decays of higher excited charm states, is in agreement with the value $\varepsilon = 0.04$ tuned by ALEPH, supporting the hypothesis of fragmentation universality between ep and e^+e^-.

The QCD models, with the fragmentation parameters fitted to the data, also provide a good description of the Q^2 and W dependence of the fragmentation observables.

The NLO calculation as implemented in HVQDIS with the Kartvelishvili fragmentation function leads to a good fit of the data, while it fails when the Peterson fragmentation function is used.

Finally, the hemisphere method is used to study the fragmentation of charm produced close to the kinematic threshold by selecting a sample of events within the visible phase space, but without a $D^{*\pm}$ jet. The description of this sample by the QCD models is not as good as in case of the nominal sample, i.e. with a $D^{*\pm}$ jet in the event. The fragmentation parameters extracted using this sample of events are significantly different from the parameters fitted to the nominal sample, which can be interpreted as an inadequacy of the QCD models and possibly of the simple parametrisations used for the fragmentation function in the phase space region close to kinematic threshold. The NLO calculation implemented in HVQDIS fails to describe the event sample without a $D^{*\pm}$ jet.

Acknowledgements

We are grateful to the HERA machine group whose outstanding efforts have made this experiment possible. We thank the engineers and technicians for their work in constructing and maintaining the H1 detector, our funding agencies for financial support, the DESY technical staff for continual assistance and the DESY directorate for support and for the hospitality which they extend to the non DESY members of the collaboration.

References

[1] R.D. Field and R.P. Feynman, "A parametrization of the properties of quark jets," Nucl. Phys. **B 136** (1978) 1.

[2] X. Artru and G. Mennessier, "String model and multiproduction," Nucl. Phys. **B 70** (1974) 93;
B. Andersson *et al.*, "Parton Fragmentation and String Dynamics," Phys. Reports **97** (1983) 31.

[3] R. Seuster *et al.* [BELLE Collaboration], "Charm Hadrons from Fragmentation and B Decays in e^+e^- Annihilation at $\sqrt{s} = 10.6$ GeV," Phys. Rev. D **73** (2006) 032002 [arXiv:hep-ex/0506068].

[4] M. Artuso *et al.* [CLEO Collaboration], "Charm Meson Spectra in e^+e^- Annihilation at 10.5 GeV c.m.e," Phys. Rev. D **70** (2004) 112001 [arXiv:hep-ex/0402040].

[5] R.A. Briere *et al.* [CLEO Collaboration], "Measurements of Charm Fragmentation into D_s^{*+} and D_s^+ in e^+e^- Annihilations at $\sqrt{s} = 10.5$ GeV," Phys. Rev. D **62** (2000) 072003 [arXiv:hep-ex/0004028].

[6] R. Barate *et al.* [ALEPH Collaboration], "Study of Charm Production in Z Decays," Eur. Phys. J. C **16** (2000) 597 [arXiv:hep-ex/9909032].

[7] R. Akers *et al.* [OPAL Collaboration], "A measurement of the production of $D^{*\pm}$ mesons on the Z^0 resonance," Z. Phys. C **67** (1995) 27.

[8] P. Abreu *et al.* [DELPHI Collaboration], "A measurement of D meson production in Z^0 hadronic decays," Z. Phys. C **59** (1993) 533 [Erratum-ibid. C **65** (1995) 709].

[9] H. Albrecht *et al.* [ARGUS Collaboration], "Inclusive production of $D0$, D^+ and $D^{*+}(2010)$ mesons in B decays and nonresonant e^+e^- annihilation at 10.6 GeV," Z. Phys. C **52** (1991) 353.

[10] D. Bortoletto *et al.* [CLEO Collaboration], "Charm Production In Nonresonant e^+e^- Annihilations at $\sqrt{s} = 10.55$ GeV," Phys. Rev. D **37** (1988) 1719 [Erratum-ibid. D **39** (1989) 1471].

[11] A. Aktas *et al.* [H1 Collaboration], "Inclusive Production of D^+, D^0, D_s^+ and D^{*+} Mesons in Deep Inelastic Scattering at HERA," Eur. Phys. J. C **38** (2005) 447 [arXiv:hep-ex/0408149].

[12] S. Chekanov *et al.* [ZEUS Collaboration], "Measurement of charm fragmentation ratios and fractions in photoproduction at HERA ," Eur. Phys. J. C **44** (2005) 351 [arXiv:hep-ex/0508019].

[13] H. Jung, "Hard diffractive scattering in high-energy ep collisions and the Monte Carlo generator RAPGAP," Comput. Phys. Commun. **86** (1995) 147; RAPGAP 3.2 program manual unpublished, http://www.desy.de/ jung/rapgap/.

[14] T. Sjostrand *et al.* "High-energy-physics event generation with PYTHIA 6.1," Comput. Phys. Commun. **135** (2001) 238 [arXiv:hep-ph/0010017];
T. Sjostrand, L. Lonnblad and S. Mrenna, "PYTHIA 6.2: Physics and manual," [arXiv:hep-ph/0108264] (here, version 6.224 was used).

[15] H. Jung and G.P. Salam, " Hadronic final state predictions from CCFM: the hadron level Monte Carlo generator CASCADE," Eur. Phys. J. **C19** (2001) 351 [arXiv:hep-ph/0012143];
H. Jung, " The CCFM Monte Carlo generator CASCADE," Comput. Phys. Commun. **143** 100 (2002) 143 [arXiv:hep-ph/0109102] (here, version 1.2008 was used).

[16] B.W. Harris and J. Smith, "Heavy quark correlations in deep-inelastic electroproduction," Nucl. Phys. B **452** (1995) 109 [arXiv:hep-ph/9503484];
B.W. Harris and J. Smith, " Invariant mass distributions for heavy quark-antiquark pairs in deep inelastic electroproduction," Phys. Lett. B **353** (1995) 535 [Erratum-ibid. B **359** (1995)] 423 [arXiv:hep-ph/9502312].

[17] I. Abt *et al.* [H1 Collaboration], "The H1 detector at Hera," Nucl. Instrum. Meth. A **386** (1997) 310;
I. Abt *et al.* [H1 Collaboration], "The Tracking, calorimeter and muon detectors of the H1 experiment at HERA," Nucl. Instrum. Meth. A **386** (1997) 348.

[18] R.D. Appuhn *et al.* [H1 SpaCal Group], "The H1 lead / scintillating fiber calorimeter," Nucl. Instrum. Meth. A **386** (1997) 397.

[19] D. Pitzl *et al.*, "The H1 silicon vertex detector," Nucl. Instrum. Meth. A **454** (2000) 334 [arXiv:hep-ex/0002044].

[20] B. Andrieu *et al.* [H1 Calorimeter Group], "The H1 liquid argon calorimeter system," Nucl. Instrum. Meth. A **336** (1993) 460.

[21] S. Aid *et al.* [H1 Collaboration], "Photoproduction of $D^{*\pm}$ Mesons in ep Collisions at HERA," Nucl. Phys. B **472** (1996) 32 [arXiv:hep-ex/9604005];
C. Adloff *et al.* [H1 Collaboration], "Measurement of D^* Meson Cross Sections at HERA and Determination of the Gluon Density in the Proton using NLO QCD," Nucl. Phys. B **545** (1999) 21 [arXiv:hep-ex/9812023];
C. Adloff *et al.* [H1 Collaboration], "Measurement of $D^{*\pm}$ Meson Production and F_2^c in Deep-Inelastic Scattering at HERA," Phys. Lett. B **528** (2002) 199 [arXiv:hep-ex/0108039];
A. Aktas *et al.* [H1 Collaboration], "Production of D^* Mesons with Dijets in Deep-Inelastic Scattering at HERA," Eur. Phys. J. C **51** (2007) 549 [arXiv:hep-ex/0701023].

[22] G.J. Feldman *et al.*, "Observation of the Decay $D^{*+} \to D^0\pi^+$," Phys. Rev. Lett. **38** (1977) 1313.

[23] S.D. Ellis and D.E. Soper, "Successive Combination Jet Algorithm for Hadron Collisions," Phys. Rev. D **48** (1993) 3160 [arXiv:hep-ph/9305266];
S. Catani *et al.* "Longitudinally invariant $k_\perp$ clustering algorithms for hadron hadron collisions," Nucl. Phys. B **406** (1993) 187.

[24] R. Brun *et al.*, GEANT 3, CERN, DD/EE/84-1, 11, Revised, 1987.

[25] V.N. Gribov and L.N. Lipatov, "Deep Inelastic ep Scattering In Perturbation Theory," Sov. J. Nucl. Phys. **15** (1972) 438 [Yad. Fiz. **15** (1972) 781];
V.N. Gribov and L.N. Lipatov, "e^+e^- Pair Annihilation And Deep Inelastic ep Scattering In Perturbation Theory," Sov. J. Nucl. Phys. **15** (1972) 675 [Yad. Fiz. **15** (1972) 1218];
L.N. Lipatov, "The parton model and perturbation theory," Sov. J. Nucl. Phys. **20** (1975) 94 [Yad. Fiz. **20** (1974) 181];
G. Altarelli and G. Parisi, "Asymptotic Freedom In Parton Language," Nucl. Phys. **B 126** (1977) 298;

Y.L. Dokshitzer, "Calculation Of The Structure Functions For Deep Inelastic Scattering And e^+e^- Annihilation By Perturbation Theory In Quantum Chromodynamics. (In Russian)," Sov. Phys. JETP **46** (1977) 641 [Zh. Eksp. Teor. Fiz. **73** (1977) 1216].

[26] M. Ciafaloni, "Coherence Effects in Initial Jets at small q^2/s," Nucl. Phys. B **296** (1988) 49;
S. Catani, F. Fiorani and G. Marchesini, "QCD Coherence In Initial State Radiation," Phys. Lett. B **234** (1990) 339;
S. Catani, F. Fiorani and G. Marchesini, "Small x Behavior of Initial State Radiation in Perturbative QCD," Nucl. Phys. B **336** (1990) 18;
G. Marchesini, "QCD coherence in the structure function and associated distributions at small x," Nucl. Phys. B **445** (1995) 49 [arXiv:hep-ph/9412327].

[27] H. Jung, "Un-integrated PDFs in CCFM," *Procs. of the XII International Workshop on Deep Inelastic Scattering (DIS 2004)*, Štrbské Pleso, Slovakia, April 14-18, 2004, Eds. D. Bruncko, J. Ferencei and P. Stríženec, IEP SAS, Košice, Vol. I, p. 299. [arXiv:hep-ph/0411287].

[28] C. Peterson, D. Schlatter, I. Schmitt and P. M. Zerwas, "Scaling Violations in Inclusive e^+e^- Annihilation Spectra," Phys. Rev. D **27** (1983) 105.

[29] V.G. Kartvelishvili, A.K. Likhoded and V.A. Petrov, "On the Fragmentation Functions of Heavy Quarks into Hadrons," Phys. Lett. B **78** (1978) 615.

[30] M.G. Bowler, "e^+e^- Production of Heavy Quarks in the String Model," Z. Phys. C **11** (1981) 169;
D.A. Morris, "Heavy Quark Fragmentation Functions in a Simple String Model," Nucl. Phys. B **313** (1989) 634.

[31] S. Schael *et al.* [ALEPH Collaboration], "Bose-Einstein correlations in W-pair decays with an event-mixing technique," Phys. Lett. B **606** (2005) 265; G. Rudolph [ALEPH Collaboration], private communication.

[32] G. Corcella *et al.*, "HERWIG 6: An event generator for hadron emission reactions with interfering gluons (including supersymmetric processes)," JHEP **0101** (2001) 010 [arXiv:hep-ph/0011363];
G. Corcella *et al.*, "HERWIG 6.5 release note," [arXiv:hep-ph/0210213].

[33] H.L. Lai *et al.* [CTEQ Collaboration], "Global QCD Analysis of Parton Structure of the Nucleon: CTEQ5 Parton Distributions," Eur. Phys. J. C **12** (2000) 375 [arXiv:hep-ph/9903282].

[34] G.A. Schuler and T. Sjostrand, "Parton Distributions of the Virtual Photon," Phys. Lett. B **376** (1996) 193 [arXiv:hep-ph/9601282].

[35] A.Höcker and V.Kartvelishvili, "SVD approach to data unfolding", Nucl. Instr. and Meth. **A 372** (1996) 469.

[36] A. Kwiatkowski, H. Spiesberger and H. J. Mohring, "Heracles: An Event Generator For ep Interactions At Hera Energies Including Radiative Processes: Version 1.0," Comput. Phys. Commun. **69** (1992) 155, (version 4.6 was used), http://www.desy.de/ hspiesb/heracles.html (here, version 4.6 was used).

[37] T. Ahmed *et al.* [H1 Collaboration], "Deep inelastic scattering events with a large rapidity gap at HERA," Nucl. Phys. B **429** (1994) 477.

parameter	ALEPH setting	default setting	description
'MSTJ(11)'	3	4	choice of fragmentation function: 3 Peterson fragmentation (for c, b) 4 Bowler fragmentation (for c, b)
'MSTJ(12)'	2	2	baryon model option
'MSTJ(46)'	0	3	parton shower azimut. corr.
'MSTJ(51)'	0	0	BEC off
'PARJ(1)'	0.108	0.100	P(qq)/P(q)
'PARJ(2)'	0.286	0.300	P(s)/P(u)
'PARJ(3)'	0.690	0.400	P(us)/P(ud)/P(s)/P(d)
'PARJ(4)'	0.050	0.050	(1/3)P(ud_1)/P(ud_0)
'PARJ(11)'	0.553	0.500	P(S=1)d,u
'PARJ(12)'	0.470	0.600	P(S=1)s
'PARJ(13)'	0.650	0.750	P(S=1)c,b
'PARJ(14)'	0.120	0.000	P(S=0,L=1,J=1) AXIAL
'PARJ(15)'	0.040	0.000	P(S=1,L=1,J=0) SCALAR
'PARJ(16)'	0.120	0.000	P(S=0,L=1,J=1) AXIAL
'PARJ(17)'	0.200	0.000	P(S=1,L=1,J=2) TENSOR
'PARJ(19)'	0.550	1.000	extra Baryon Suppression
'PARJ(21)'	0.366	0.360	σ_q
'PARJ(25)'	1.000	1.000	extra η suppression
'PARJ(26)'	0.276	0.400	extra η' suppression
'PARJ(41)'	0.400	0.300	Lund symm. fragm.: a
'PARJ(42)'	0.885	0.580	Lund symm. fragm.: b
'PARJ(54)'	-0.040	-0.050	ε_c
'PARJ(55)'	-0.002	-0.005	ε_b
'PARJ(82)'	1.390	1.000	Q_0
'PARP(72)'	0.295	0.250	Λ for α_s in time-like parton showers

Table 4: PYTHIA parameter settings: shown are three settings, the one from ALEPH [31], the default setting of PYTHIA (version 6.2) [14] with the BOWLER fragmentation function, and the default setting but with the Peterson fragmentation function (differs from the previous one only in the value of MSTJ(11)). The first setting is used for detector corrections, and all three are used for the predictions which in figure 4 are compared with data. Finally, the first and the last settings are used in the procedure to extract optimal fragmentation function parameters.

bin in z_{hem}	normalised cross section	statistical error	uncorrelated systematic error	correlated systematic errors positron energy	hadronic scale	beauty	total error
[0.2-0.4[	0.93	0.11	0.02	-0.008	-0.027	-0.020	0.11
[0.4-0.5[	1.53	0.13	0.03	-0.014	-0.037	-0.019	0.14
[0.5-0.625[	1.80	0.15	0.03	+0.002	-0.032	+0.007	0.15
[0.625-0.75[	1.85	0.14	0.03	+0.008	+0.030	+0.019	0.15
[0.75-0.85[	1.27	0.11	0.02	+0.008	+0.056	+0.016	0.13
[0.85-1.0]	0.52	0.06	0.01	+0.010	+0.025	+0.007	0.07

Table 5: Normalised $D^{*\pm}$ meson differential cross section as a function of z_{hem}, in the visible phase space described in section 7, including the requirement of a $D^{*\pm}$ jet in the event. The data are normalised to unity in the given range of z_{hem}. All errors are considered to be symmetric in each bin, for correlated systematic errors a relative sign is indicated.

bin in z_{jet}	normalised cross section	statistical error	uncorrelated systematic error	correlated systematic errors positron energy	hadronic scale	beauty	total error
[0.3-0.55[	0.61	0.10	0.01	-0.005	-0.029	-0.016	0.10
[0.55-0.7[	1.76	0.15	0.03	-0.001	-0.026	+0.004	0.16
[0.7-0.825[	2.17	0.18	0.04	+0.009	+0.032	+0.017	0.19
[0.825-0.9[	1.47	0.18	0.03	-0.011	+0.043	+0.004	0.19
[0.9-1.0]	2.03	0.17	0.04	+0.012	+0.038	+0.011	0.18

Table 6: Normalised $D^{*\pm}$ meson differential cross section as a function of z_{jet}, in the visible phase space described in section 7, including the requirement of a $D^{*\pm}$ jet in the event. The data are normalised to unity in the given range of z_{jet}. All errors are considered to be symmetric in each bin, for correlated systematic errors a relative sign is indicated.

RAPGAP with PYTHIA parameter settings	fragmentation function	hemisphere observable (χ^2/n.d.f.)	jet observable (χ^2/n.d.f.)
Aleph	Peterson $\varepsilon = 0.04$	6.0/5	4.3/4
default	Peterson $\varepsilon = 0.05$	6.1/5	6.0/4
default	Bowler $a = 0.3, b = 0.58$	5.6/5	3.5/4

Table 7: The parameter settings used for the RAPGAP predictions and χ^2/n.d.f. as calculated from them and the data.

model	α Kartvelishvili (χ^2/n.d.f.)		ε Peterson (χ^2/n.d.f.)	
	hemisphere	jet	hemisphere	jet
PYTHIA default parameter setting:				
RAPGAP	$\alpha = 3.3^{+0.4}_{-0.4}$ (1.9/4)	$\alpha = 3.1^{+0.3}_{-0.3}$ (2.3/3)	$\varepsilon = 0.049^{+0.012}_{-0.010}$ (6.1/4)	$\varepsilon = 0.061^{+0.011}_{-0.009}$ (4.4/3)
CASCADE	$\alpha = 3.5^{+0.4}_{-0.4}$ (2.4/4)	$\alpha = 3.2^{+0.3}_{-0.3}$ (3.5/3)	$\varepsilon = 0.044^{+0.012}_{-0.009}$ (7.1/4)	$\varepsilon = 0.060^{+0.010}_{-0.009}$ (5.0/3)
PYTHIA with ALEPH parameter setting:				
RAPGAP	$\alpha = 4.5^{+0.6}_{-0.5}$ (3.4/4)	$\alpha = 4.3^{+0.4}_{-0.4}$ (3.1/3)	$\varepsilon = 0.029^{+0.007}_{-0.005}$ (4.8/4)	$\varepsilon = 0.035^{+0.007}_{-0.006}$ (4.1/3)
CASCADE	$\alpha = 4.5^{+0.6}_{-0.5}$ (2.6/4)	$\alpha = 4.4^{+0.4}_{-0.4}$ (2.6/3)	$\varepsilon = 0.027^{+0.007}_{-0.005}$ (4.0/4)	$\varepsilon = 0.034^{+0.007}_{-0.006}$ (3.7/3)
fixed-order (NLO) calculation:				
HVQDIS	$\alpha = 3.3^{+0.4}_{-0.4}$ (4.8/4)	$\alpha = 3.8^{+0.3}_{-0.3}$ (5.0/3)	$\varepsilon = 0.070^{+0.015}_{-0.013}$ (19.8/4)	$\varepsilon = 0.034^{+0.004}_{-0.004}$ (24.0/3)

Table 8: Fragmentation function parameters extracted for the QCD models of RAPGAP and CASCADE, with the parameter settings as summarised in table 4, and for the NLO QCD program HVQDIS, using the hemisphere and jet observables in the visible phase space described in section 7, including the requirement of a $D^{*\pm}$ jet in the event.

bin in z_{hem}	normalised cross section	statistical error	uncorrelated systematic error	correlated systematic errors positron energy	hadronic scale	beauty	total error
[0.2-0.4[	0.50	0.09	0.01	+0.003	-0.017	-0.007	0.09
[0.4-0.5[	0.97	0.12	0.01	+0.004	-0.023	-0.009	0.12
[0.5-0.625[	1.44	0.16	0.01	-0.006	-0.026	-0.002	0.16
[0.625-0.75[	1.77	0.17	0.02	-0.016	-0.005	+0.005	0.17
[0.75-0.85[	2.13	0.15	0.02	+0.008	+0.037	+0.009	0.16
[0.85-1.0]	1.26	0.10	0.01	+0.006	+0.038	+0.006	0.11

Table 9: Normalised $D^{*\pm}$ meson differential cross section as a function of z_{hem}, in the visible phase space described in section 7, but with the requirement that there is no $D^{*\pm}$ jet in the event. The data are normalised to unity in the given range of z_{hem}. All errors are considered to be symmetric in each bin, for correlated systematic errors a relative sign is indicated.

hemisphere observable, events without $D^{*\pm}$ jet		
model	α Kartvelishvili (χ^2/n.d.f.)	ε Peterson (χ^2/n.d.f.)
PYTHIA default parameter setting:		
RAPGAP	$\alpha = 7.6^{+1.3}_{-1.1}$ $(6.1/4)$	$\varepsilon = 0.010^{+0.003}_{-0.002}$ $(4.2/4)$
CASCADE	$\alpha = 6.9^{+1.0}_{-0.9}$ $(4.3/4)$	$\varepsilon = 0.014^{+0.004}_{-0.003}$ $(3.1/4)$
PYTHIA with ALEPH parameter setting:		
RAPGAP	$\alpha = 10.3^{+1.7}_{-1.6}$ $(3.0/4)$	$\varepsilon = 0.006^{+0.002}_{-0.002}$ $(1.7/4)$
CASCADE	$\alpha = 8.2^{+1.2}_{-1.1}$ $(5.2/4)$	$\varepsilon = 0.011^{+0.003}_{-0.002}$ $(4.9/4)$
fixed-order (NLO) calculation:		
HVQDIS	$\alpha = 6.0^{+1.0}_{-0.8}$ $(44.2/4)$	$\varepsilon = 0.007^{+0.001}_{-0.001}$ $(42.6/4)$

Table 10: Fragmentation function parameters extracted for the QCD models of RAPGAP and CASCADE, with parameter settings as summarised in table 4, and for the NLO QCD program HVQDIS, in the visible phase space described in section 7, but with the requirement that there is no $D^{*\pm}$ jet in the event.

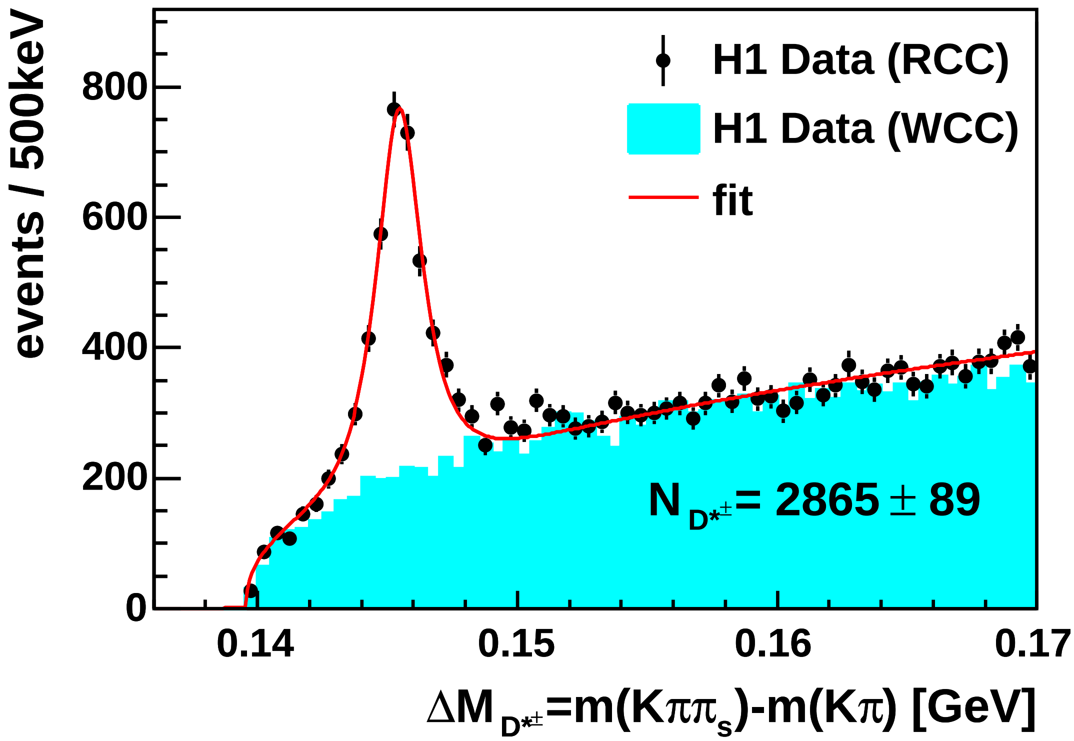

Figure 1: Distributions of $\Delta M_{D^{*\pm}} = m(K\pi\pi_s) - m(K\pi)$ for right charge combinations (RCC) and for wrong charge $K\pi$ combinations (WCC) in the accepted D^0 mass window.

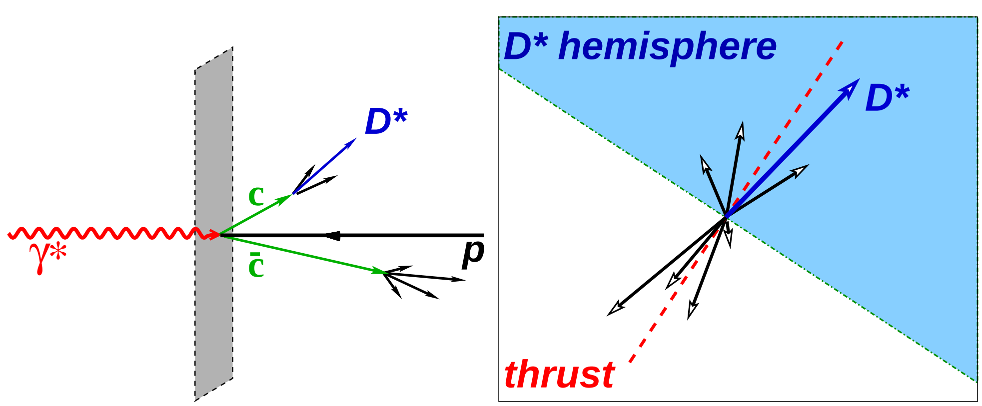

Figure 2: Illustration of the hemisphere method: a $c\bar{c}$ pair in the $\gamma^* p$-rest-frame (left) and in a plane perpendicular to the photon momentum (right).

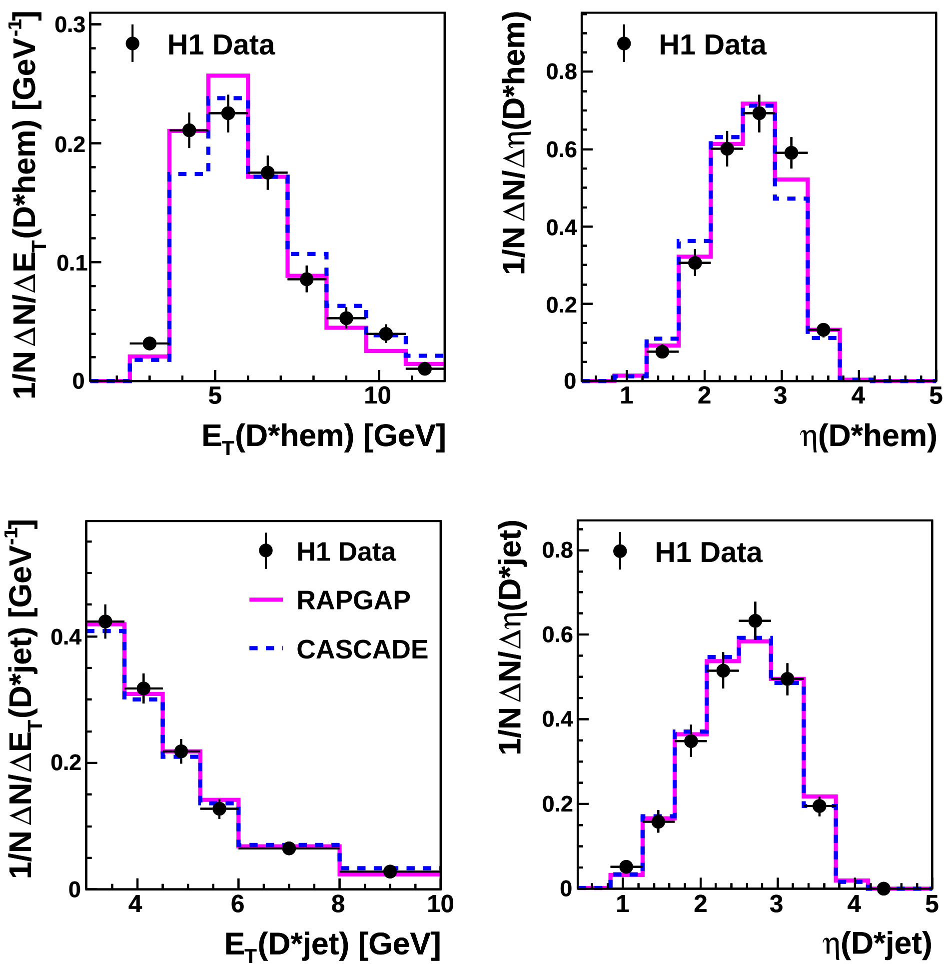

Figure 3: Comparison on detector level between data and Monte Carlo models used to correct the data for detector effects. Shown are E_{T}^{*} and η^{*} of the $D^{*\pm}$ meson hemisphere and E_{T}^{*} and η^{*} of the $D^{*\pm}$ jet. All observables are calculated in the $\gamma^{*}p$-rest-frame.

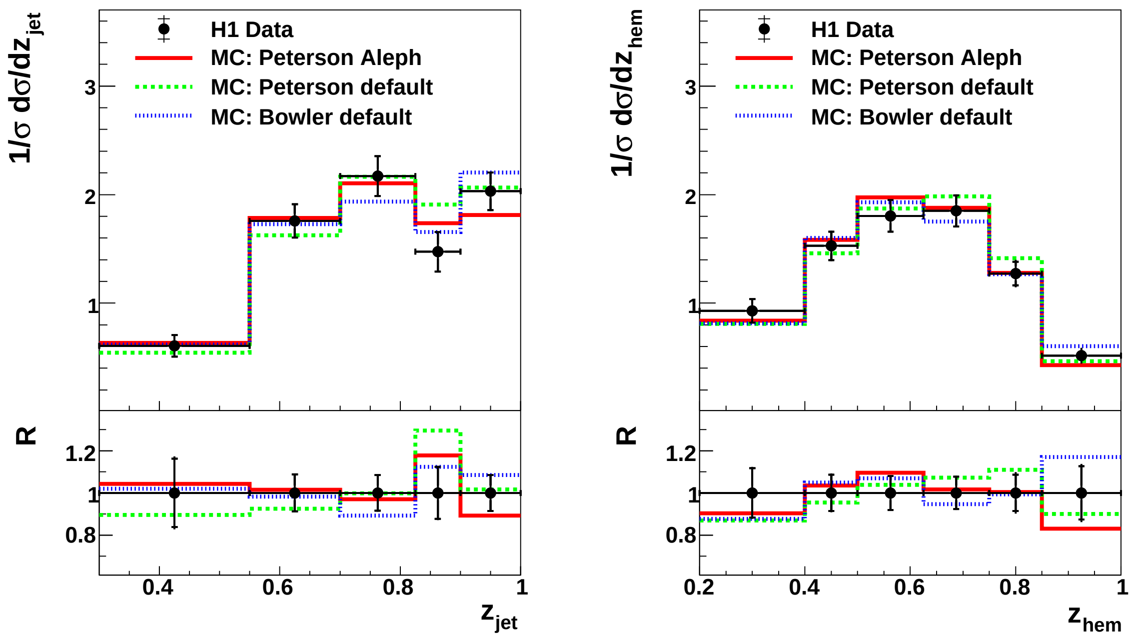

Figure 4: Normalised $D^{*\pm}$ meson cross sections as a function of $\mathrm{z_{jet}}$ and $\mathrm{z_{hem}}$ (sample of events with a $D^{*\pm}$ jet in the event). The distributions are normalised to unity in the displayed range of $\mathrm{z_{jet}}$ and $\mathrm{z_{hem}}$ respectively. The data are compared with MC predictions of RAPGAP, using PYTHIA default settings with Peterson or Bowler parametrisations and the ALEPH setting, which includes the production of higher excited charm states (see table 4). The ratio $\mathrm{R = MC/data}$ is shown as well as the relative statistical uncertainties (inner error bars) and the relative statistical and systematic uncertainties added in quadrature (outer error bars) for the data points at $\mathrm{R} = 1$.

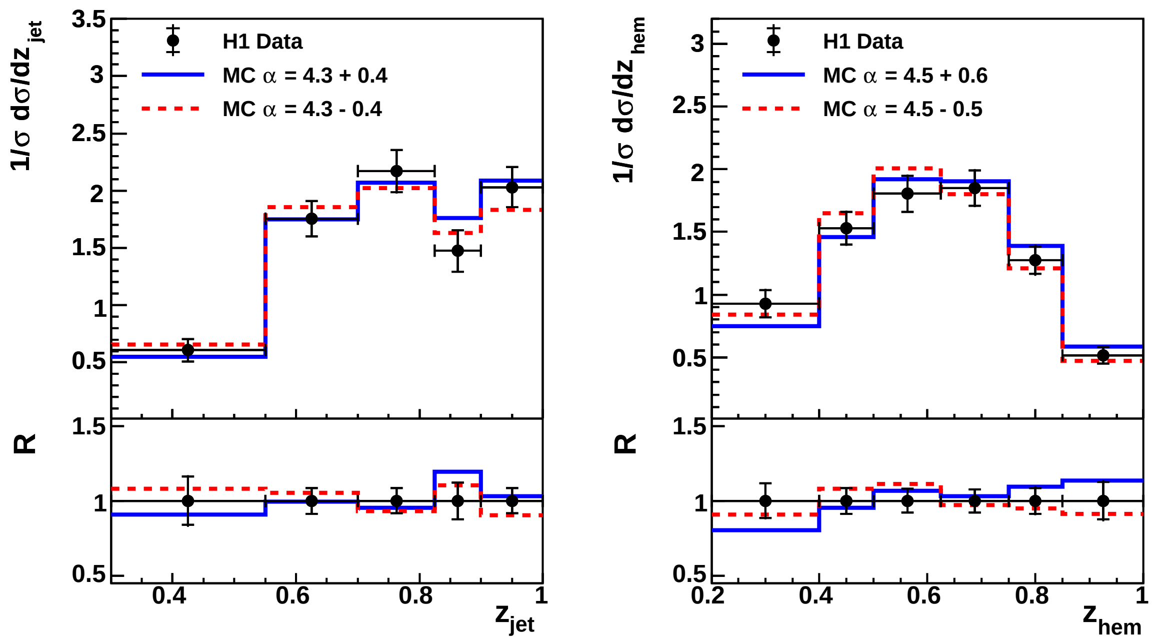

Figure 5: Normalised $D^{*\pm}$ meson cross sections as a function of $\mathrm{z_{jet}}$ and $\mathrm{z_{hem}}$ (sample of events with a $D^{*\pm}$ jet in the event). They are normalised to unity in the displayed range of $\mathrm{z_{jet}}$ and $\mathrm{z_{hem}}$ respectively. The same data as in figure 4 are compared with the predictions of the MC program RAPGAP using the ALEPH setting and Kartvelishvili parametrisation. The fragmentation function parameter α is fitted according to the procedure described in section 7. The full and dashed line indicate a variation of the fragmentation parameter by $\pm 1\sigma$ around the best fit value of α. The ratio $\mathrm{R} = \mathrm{MC/data}$ is described in the caption of Fig. 4.

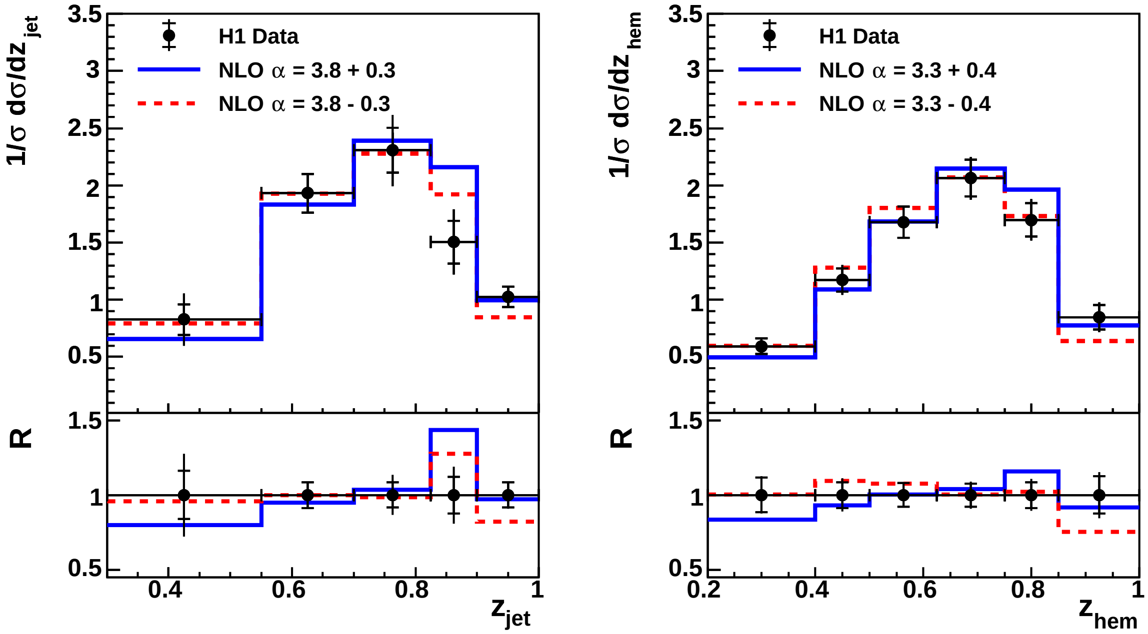

Figure 6: Normalised $D^{*\pm}$ meson cross sections as a function of $\mathrm{z_{jet}}$ and $\mathrm{z_{hem}}$ (sample of events with a $D^{*\pm}$ jet in the event). The data are corrected for hadronisation effects (see section 5). They are normalised to unity in the displayed range of $\mathrm{z_{jet}}$ and $\mathrm{z_{hem}}$ respectively. The data are compared with NLO predictions of HVQDIS using the Kartvelishvili parametrisation. The fragmentation function parameter α is fitted according to the procedure described in section 7. The full and dashed line indicate a variation of the fragmentation parameter by $\pm 1\sigma$ around the best fit value of α. The ratio $\mathrm{R = MC/data}$ is described in the caption of Fig. 4.

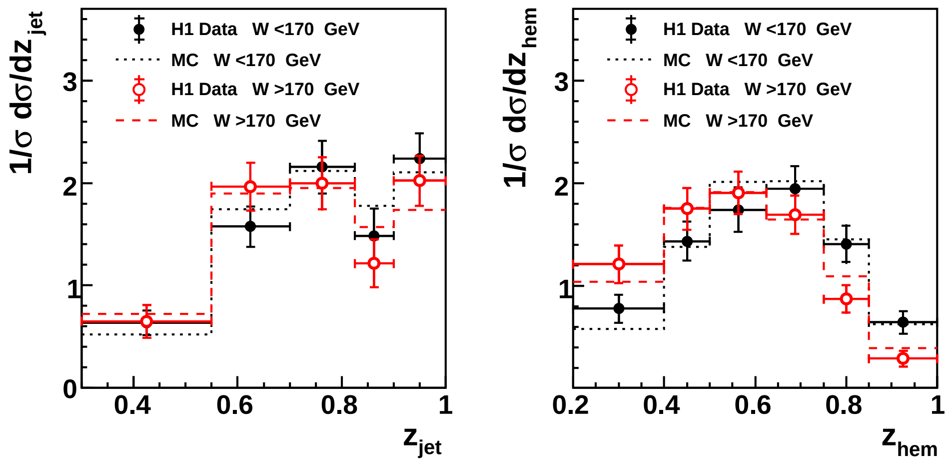

Figure 7: Normalised $D^{*\pm}$ meson cross sections as a function of $\mathrm{z_{hem}}$ and $\mathrm{z_{jet}}$ for $W < 170$ and $W > 170$ GeV, (sample of events with a $D^{*\pm}$ jet in the event). The cross sections are normalised to unity in the displayed range of $\mathrm{z_{jet}}$ and $\mathrm{z_{hem}}$ respectively. In addition, the MC predictions of RAPGAP are shown using the ALEPH setting and the optimised fragmentation parameters α for the Kartvelishvili parametrisation as given in table 8 for $\mathrm{z_{jet}}$ and $\mathrm{z_{hem}}$.

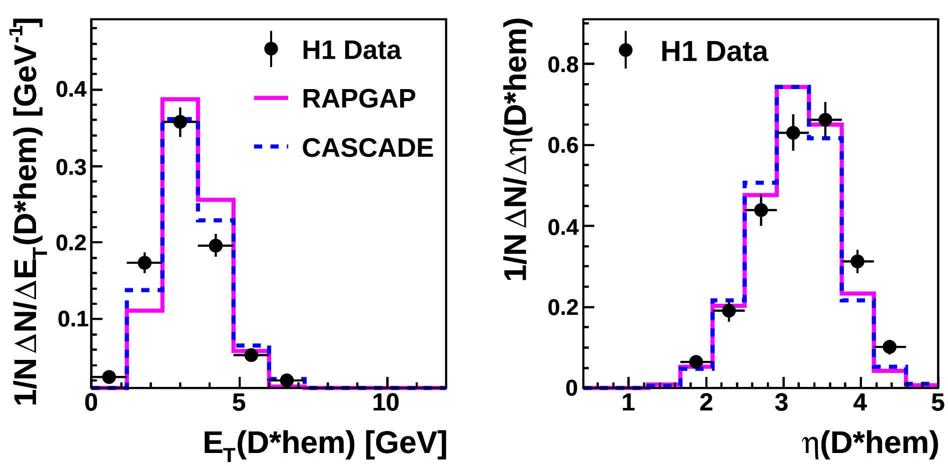

Figure 8: Comparison on detector level between data and Monte Carlo models used to correct the data for detector effects for the sample of events requiring that there is no $D^{*\pm}$ jet in the event (see section 7.2). Shown are E_{T}^{*} and η^{*} of the $D^{*\pm}$ meson hemisphere. All quantities are calculated in the $\gamma^{*}p$-rest-frame.

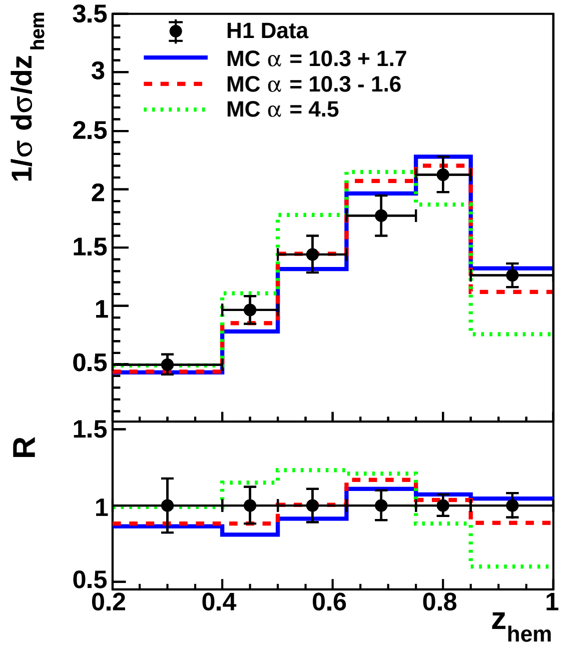

Figure 9: Normalised $D^{*\pm}$ meson cross sections as a function of $\mathrm{z_{hem}}$ for the sample of events requiring that there is no $D^{*\pm}$ jet in the event. They are normalised to unity in the displayed range of $\mathrm{z_{hem}}$. The data are compared with MC predictions of RAPGAP using the ALEPH setting and Kartvelishvili fragmentation function. The fragmentation parameter α is fitted according to the procedure described in section 7. The full and dashed line indicate a variation of the fragmentation parameter by $\pm 1\sigma$ around the best fit value of α. The green dashed line shows the prediction of RAPGAP with the fragmentation parameter α extracted from the nominal data sample. The ratio $\mathrm{R = MC/data}$ is described in the caption of Fig. 4.